



# HydroGFD3.0: a 25 km global near real-time updated precipitation and temperature data set

Peter Berg<sup>1</sup>, Fredrik Almén<sup>1</sup>, and Denica Bozhinova<sup>1</sup>

<sup>1</sup>Swedish Meteorological and Hydrological Institute, Folkborgsvägen 17, 601 76 Norrköping, Sweden

**Correspondence:** Peter Berg (peter.berg@smhi.se)

1 **Abstract.** HydroGFD (Hydrological Global Forcing Data) is a data set of bias adjusted reanalysis data for daily precipitation,  
2 and minimum, mean, and maximum temperature. It is mainly intended for large scale hydrological modeling, but is also  
3 suitable for other impact modeling. The data set has an almost global land area coverage, excluding the Antarctic continent, at  
4 a horizontal resolution of 0.25°, i.e. about 25 km. It is available for the complete ERA5 reanalysis time period; currently 1979  
5 until five days ago. This period will be extended back to 1950 once the back catalogue of ERA5 is available. The historical  
6 period is adjusted using global gridded observational data sets, and to acquire real-time data, a collection of several reference  
7 data sets is used. Consistency in time is attempted by relying on a background climatology, and only making use of anomalies  
8 from the different data sets. Precipitation is adjusted for mean bias as well as the number of wet days in a month. The latter is  
9 relying on a calibrated statistical method with input only of the monthly precipitation anomaly, such that no additional input  
10 data about the number of wet days is necessary. The daily mean temperature is adjusted toward the monthly mean of the  
11 observations, and applied to 1 h timesteps of the ERA5 reanalysis. Daily mean, minimum and maximum temperature are then  
12 calculated. The performance of the HydroGFD3 data set is on par with other similar products, although there are significant  
13 differences in different parts of the globe, especially where observations are uncertain. Further, HydroGFD3 tends to have  
14 higher precipitation extremes, partly due to its higher spatial resolution. In this paper, we present the methodology, evaluation  
15 results, and how to access to the data set at doi:10.5281/zenodo.3871707.

## 16 1 Introduction

17 Precipitation ( $P$ ) and temperature ( $T$ ) are key driving parameters for many impact models, and there are now many observa-  
18 tional data sets available. They differ regarding the spatio-temporal resolution, the historical coverage, and the data sources  
19 included in the product. However, when it comes to continuously updated near real-time data sets, there are very few available  
20 data sets. It is therefore challenging to find a product suitable for monitoring and initialization of forecasts for an impact model,  
21 i.e. a product that fulfills both a long historical period for calibration and validation, as well as real-time updates.

22 While most data sets now offer a rather long historical period, the real-time availability is a greater challenge. Merged  
23 satellite and gauge data sets such as CHIRPS (Funk et al., 2015a), CMORPH (Joyce et al., 2004), and PERSIANN-CDR  
24 (Ashouri et al., 2015) offer both high resolution and near-realtime components, but are limited to between the +/-50 or +/-60  
25 degree latitude bands. Several data sets have made use of reanalysis data as a basis, adjusted using various gridded observational



26 data sets (Weedon et al., 2011, 2014; Beck et al., 2017; Berg et al., 2018). The advantage is that the reanalysis products are  
27 readily available with a large range of variables and output frequencies. Still, the downside with reanalysis products is that  
28 especially  $P$  is a model product and thereby suffers from model bias. Since the bias can be substantial, several methods have  
29 been developed to adjust reanalysis, using different methods and reference data sets.

30 A hydrological operational monitoring or forecast product has strong demands on availability and redundancy of the data  
31 flows. The data set HydroGFD1 (Berg et al., 2018) was constructed and made operational for initializations of the hydrological  
32 model HYPE (Lindström et al., 2010) for different set-ups across the globe. It offered near-realtime updating of daily  $P$  and  
33 daily  $T$  (mean, minimum, and maximum), until the end of the last calendar month. The real-time components of HydroGFD1  
34 were based on ERA-Interim reanalysis, extended by the ECMWF deterministic forecasts, adjusted using monthly mean  $P$   
35 from GPCC-Monitoring and GPCC-FirstGuess (Schneider et al., 2018b) products, and monthly mean  $T$  from GHCN-CAMS  
36 (Fan and Van den Dool, 2008). The follow-up data set HydroGFD2 offered some updates to the methodology, and shifted  
37 to using primarily the CPC-Unified (Chen et al., 2008) and CPC-Temp (CPCtemp, 2017) products for  $P$  and  $T$  adjustments,  
38 respectively. Both data sets have been operationally produced for a few years now, and we have identified some serious issues  
39 regarding the availability of required data sets for successful updates. The largest operational intermission occurred during the  
40 government lock-down in the US between the 22<sup>nd</sup> of December 2018 and the 25<sup>th</sup> of January 2019. Neither of the US data  
41 sets included in the production were available, which hampered the production of the HydroGFD data sets, and subsequently  
42 deteriorated the quality of some operational HYPE models. Both these HydroGFD versions have now become obsolete for  
43 real-time production due to the discontinuation of the ERA-Interim production as of August 2019. Data sets using multiple  
44 input data sources are less sensitive to such conditions, such as the MSWEP data set (Beck et al., 2017).

45 In this paper, the HydroGFD3.0 system is described, with its range of produced data sets for the period 1979 to near real-  
46 time, at  $0.25^\circ$  resolution and global land coverage. We describe the methodology and the operational production, as well as an  
47 evaluation of the climatological data set, with comparison to other similar data sources.

## 48 2 Data

49 Table 1 lists the data sources used in the production of the different *tiers* (see Methods section) of HydroGFD3. From now  
50 on, we will use the shortened internal abbreviations listed under "Name" in Tab. 1 when we refer to the data of  $P$  or  $T$  from  
51 each source. ERA5 is the latest global reanalysis product of the ECMWF (Hersbach et al., 2020) and forms the basis for  
52 HydroGFD3. This reanalysis product is chosen because our operational forecasts at SMHI are based on the medium range  
53 forecasts of ECMWF, with a similar model as that used for ERA5. Other reanalysis products would be possible, but are not  
54 explored here. ERA5 is updated with a three months lag, but a new temporary product, ERA5T, is produced with a five days  
55 lag.

56 The HydroGFD3 background climatology is based on cpct for  $T$ , and CHPclim (Funk et al., 2015b) and gpcc (Schneider  
57 et al., 2018a) for  $P$ . For the historical period, HydroGFD3 utilizes the data set CRUts4.03 (Harris and Jones, 2019) for  $T$  and  
58 wet day frequency, and gpcc for  $P$ . Several tiers are performed for the near real-time updating using different input data sets,



**Table 1.** Table of model and data sources used in the production of HydroGFD3, as well as the WFDE5 data set used for comparison. Note the lower case abbreviations used in the main text and in figures which follow the internal notation used in the data set production.

Data set	Name	Variables	Resolution	Period	Reference
ERA5	e5	$T, P$	hourly; $0.33^\circ$	1979–(t-3 months)	Hersbach et al. (2020)
ERA5T	e5t	$T, P$	hourly; $0.33^\circ$	(t-3 months) – (t-5 days)	Hersbach et al. (2020)
CRUts4.03	cru	$T, P, N_{wet}$	monthly; $0.5^\circ$	1901–(t-2 months)	Harris and Jones (2019)
GPCCv8	gpcch	$P$	monthly; $0.25^\circ$	1891–2016	Schneider et al. (2018a)
GPCC-monitoringv6	gpccm	$P$	monthly; $1.0^\circ$	1982–(t-3 months)	Schneider et al. (2018b)
GPCC-First guess	gpccf	$P$	monthly; $1.0^\circ$	2004–(t-1 month)	Schneider et al. (2018b)
CPC-Unified	cpcp	$P$	daily; $0.5^\circ$	1979–(t-2 days)	Chen et al. (2008)
CPC-Temp	cpct	$T_{min}, T_{max}$	daily; $0.5^\circ$	1979–(t-2 days)	CPCtemp (2017)
CHPclimv1.0	chpclim	$P$	climatology; $0.05^\circ$	(1980–2009)	Funk et al. (2015b)
WFDE5-CRU	wfd-cru	$T, P$	hourly; $0.5^\circ$	1979-2018	Cucchi et al. (2020)
WFDE5-GPCC	wfd-gpcc	$P$	hourly; $0.5^\circ$	1979-2016	Cucchi et al. (2020)

59 for redundancy. For  $P$ , there are products based on gpccm (Schneider et al., 2018b), gpccf (Schneider et al., 2018b), cpcp  
 60 (Chen et al., 2008), as well as a climatological adjustment. For  $T$ , there is only the cpct data set (CPCtemp, 2017), and the  
 61 climatological adjustment.

62 The analysis is comparing the different data sets included in the processing, and additionally makes use of the latest version  
 63 of the *WATCH forcing data* WFDE5 (Cucchi et al., 2020) as a state-of-the-art comparison.

### 64 3 Method

65 The main method that HydroGFD is building on consists of adding observational monthly anomalies to a background clima-  
 66 tology, then adjusting the reanalysis data to that absolute monthly mean. Further steps assure consistency between different  
 67 versions of the data set, e.g. regarding spatial coverage. The different steps in producing the HydroGFD3 data sets are presented  
 68 in detail in the following sections.

#### 69 3.1 Climatology

70 The  $P$  background climatology is based on the CHPclim high resolution climatology of satellite, gauge, and physiographic  
 71 indicators (Funk et al., 2015b). We retain the same climatological period throughout the HydroGFD3 data set. CHPclim comes  
 72 in two versions, one with full coverage for the  $50^\circ\text{S}$ – $50^\circ\text{N}$  latitude band, and one with global land coverage. We choose to  
 73 make the global coverage version the main choice, but add information from the tropical full coverage version to increase  
 74 coverage along coastlines and islands. The original  $0.05^\circ$  resolution is remapped conservatively to the  $0.25^\circ$  resolution of  
 75 the HydroGFD3 dataset. Some issues with the CHPclim data set were identified, with observational artifacts in mid-northern



76 Siberia, and underestimation in Scandinavia. Therefore, these two regions were replaced by GPCCV8 climatological data for  
77 the 1980–2009 period (see supplementary material for details). To avoid introducing sharp borders, a zone of five grid points  
78 were used around each area as a linear transition from one data set to another. Since Greenland  $P$  is poorly mapped by both  
79 satellite and gauge data, we have chosen to let its climatology be defined by e5, rather than any of the data sets.

80 For  $T$ , we use the cpct climatology (1980–2009) with only a remapping to the 0.25 degree resolution, and in-filling of  
81 missing data points using e5. The third climatology consists of the wet day frequency (1980–2009), which is taken from the  
82 CRUts4.03 data set of gridded station observations of the number of wet days in a month.

83 In a final step, the three climatologies are harmonized by only retaining the grid points that are available consistently in all  
84 data sets and all months. This leads also to the final land-mask of the HydroGFD3 data set.

85 The elevation is defined by the e5 surface geopotential divided by the gravity of Earth ( $9.80665 \text{ m/s}^2$ ).

### 86 3.2 Anomaly method

87 HydroGFD3 makes use of several different data sets, which need to be stitched together in different configurations depending  
88 on the use. Without some kind of homogenization between the data sets, sharp changes in the data are unavoidable when  
89 switching from one data set to another. The homogenization used here is performed by only making use of anomalies from the  
90 different data sets.

91 In the earlier version HydroGFD1 (Berg et al., 2018), which is closely based on the WFD method (Weedon et al., 2011), each  
92 month of the reanalysis data set is adjusted with the absolute monthly mean of the observational data set. This main principle is  
93 retained, however, in a new homogenization step we create new absolute observations by first calculating the monthly anomaly  
94 compared to the 1989–2009 climatological period calculated for each data set, then adding this anomaly to the HydroGFD3  
95 climatology. Anomalies are additive for  $T$

$$96 \quad T_{anom}(year, month) = T(year, month) - T_{clim}(month) \quad (1)$$

97 and multiplicative for  $P$

$$98 \quad P_{anom}(year, month) = P(year, month) / P_{clim}(month) \quad (2)$$

99 The reverse operation is applied after replacing the climatology.

### 100 3.3 Wetday frequency

101 A common issue with coarse resolution models, such as e5, is a tendency to produce excessive drizzle that reduces the number  
102 of dry days in a month. To alleviate potential excessive drizzle, the number of wet days are adjusted before correcting the  $P$   
103 amount. The wetday frequencies in a month are not well covered by observational monitoring records and the uncertainties are  
104 large when available. We have chosen to estimate the number of wet days based on the method of Stillman and Zeng (2016).  
105 The method essentially relates the number of wet days,  $N_{wet}$ , to the monthly  $P$  anomaly,  $P_{anom}$ , using also the climatological

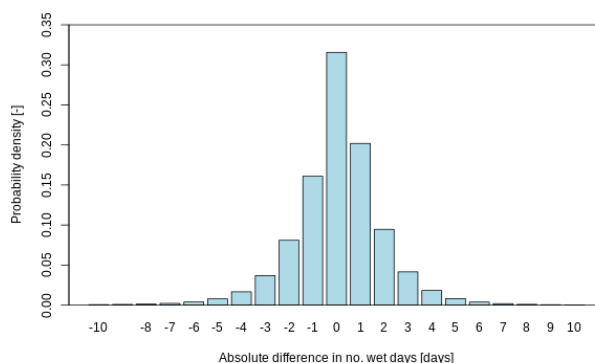


**Figure 1.** Distribution of the absolute difference in the number of wet days  $N_{wet}$  estimated through the Stillman and Zeng (2016) method, and gpch  $P$ . The probability density function ranges globally over all land grid points.

106 wet day frequency,  $N_{wet}^{clim}$  as a predictor, and a tunable constant,  $k$ .

$$107 \quad N_{wet} = P_{anom}^k * N_{wet}^{clim} \quad (3)$$

108 A value of  $k = 0.28$  was derived for HydroGFD2.0 by calibration to the cru observations of the number of wet days in a  
109 month, together with the cpcp  $P$  observations. This value is almost half of that found by Stillman and Zeng (2016), which can  
110 probably be related to the data sets used, but was found to be well applicable across the world. A verification of this constant  
111 was performed with the cru wet days and the gpch monthly  $P$  anomalies, see Fig.1. This reveals an overall high accuracy of  
112 the method, with deviations from observations of mostly only few days in a month, but can in rare cases be as much as ten  
113 days. On average over the 1980–2009 period, and for each single grid point, the deviations are close to zero. Thus, the method  
114 works well across all areas, and with sufficient precision for our purposes.

### 115 3.4 Applied corrections

116 The production of the corrected data consists of the following steps.

- 117 1. Calculate observed anomalies
- 118 2. Construct absolute reference data by adding the anomalies to the HydroGFD3 climatology
- 119 3. ( $P$  only) Calculate the number of wet days
- 120 4. ( $P$  only) Remove the weakest excessive wet days in e5
- 121 5. Calculate the ratio between the monthly means of the reference and e5
- 122 6. Apply the ratio to all time steps of e5

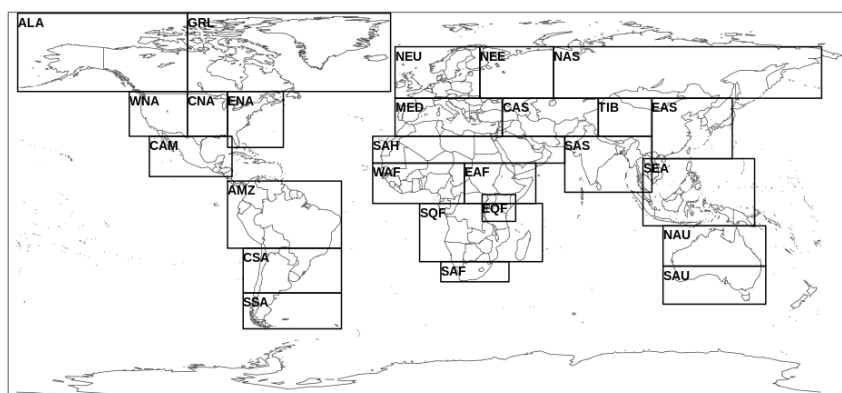


**Figure 2.** Evaluation regions as defined by Giorgi and Bi (2005), and employed in the PDF and time series analysis.

123 7. (*T* only) Calculate mean, minimum, and maximum *T* from the hourly time steps

124 For *P*, the scaling can cause very large values in some cases, e.g. when *e5* severely underestimates the number of wet days.  
125 Therefore, *P* is limited to a maximum of 1500 mm/day, which is close to the highest observed record at that time scale.

### 126 3.5 Consistency in time and space

127 To have consistent output in all version of HydroGFD3, there are internal checks to verify that each of the defined grid points  
128 of HydroGFD3 is receiving data after each monthly adjustment. It happens that the land sea mask of the observational data sets  
129 change over time, and they often differ between different data sources. If the anomaly data are not defined for a particular grid  
130 point, a search algorithm will identify if there are defined anomalies in grid points within a 5 grid box radius. If the search is  
131 successfully finding at least one value, the mean of all values in the search radius will be filling the grid point value. However,  
132 if no defined data is found, the anomaly will be set to 0 for *T* and 1 for *P*; in other words, the output will resort to adjustment  
133 toward the HydroGFD3 climatology.

### 134 3.6 Evaluation

135 Evaluation of the HydroGFD3 historical data set is presented for the mean climatology of *P* and *T*, as well as for regional  
136 probability distribution functions (PDF) of daily data and as monthly mean time series. The two latter evaluations are performed  
137 for each of the regions defined by Giorgi and Bi (2005) (although we use the correct longitude and latitude coordinates provided  
138 by Huebener and Körper (2013)) commonly referred to as Giorgi regions, see Fig. 2. One exception is that we have left out the  
139 EQF region in the plots of PDFs, since it is contained in other included regions. The reason is that it overlaps other regions,  
140 and having only 25 regions simplifies the presentation layout of the plots substantially. For both the PDFs and the time series,

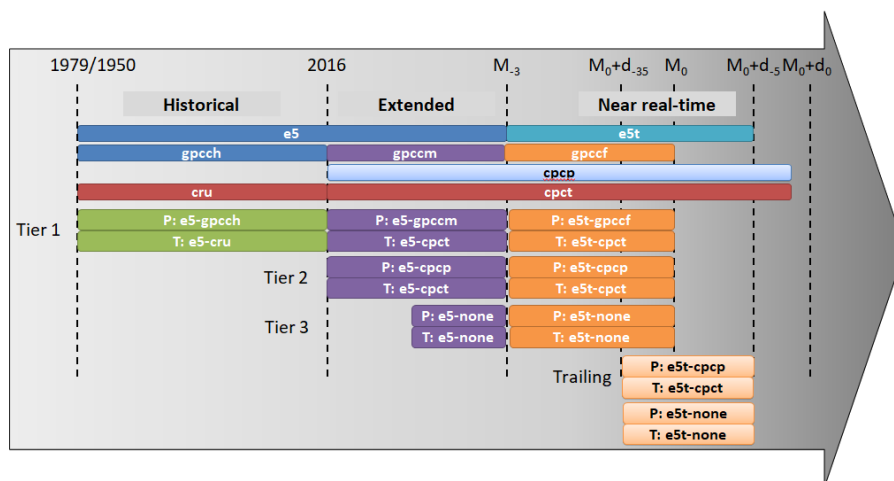


**Figure 3.** Schematic of the different HydroGFD3 products on a non-linear time axis. The top bars show the original data sources, and the Tier 1–3 and Trailing products are shown below. Abbreviations follow Tab. 1. The time axis denotes years with significant changes in data sources, and the later time marks are relative to the 1<sup>st</sup> of the current month,  $M_0$ , and the current day,  $d_0$ . The units of the sub-script for the month is in months, and for the day is in days.

141 only data points in the defined grid points of HydroGFD3 are used. The PDFs are pooling all data in each domain, whereas the  
 142 time series plots are based on regional averages for each monthly time step.

#### 143 4 Data sets

144 HydroGFD3 is built up by different data sets depending on the time period and the tier, see schematic in Fig. 3.

145 The historical period (1979–2016) is built on e5 corrected with the gpch and cru data sets, respectively for  $P$  and  $T$ .  
 146 There is only one tier produced for this period. e5 will later be released back to 1950, and the HydroGFD3 historical data will  
 147 then cover that period as well.

148 After 2016, in the "extended" and "near real-time" periods, there are three tiers built on different data sets. Tier 1 is the  
 149 primary choice and follows the gpccm (for the e5 period) and gpccf (for the e5t period) products for  $P$  adjustments, and the  
 150 cpct product (for the complete period) is used for  $T$ . Tier 2 builds instead on the cpccp and cpct products. Note that the Tier 1  
 151 and Tier 2  $T$  products are identical, and are only repeated here for simplification of the schematic. In practice, there is no Tier  
 152 2 for  $T$ , and the tiers are anyway not necessarily used consistently for  $T$  and  $P$  together, since the data sets are completely  
 153 independent. Tier 3 is the final resort if none of the data sets for a variable is available. It is performing only a climatological  
 154 correction of e5 or e5t by calculating anomalies of the reanalysis and adding/multiplying this to the HydroGFD3 climatology.  
 155 Since it does not make use of any observational data sets, it has received the internal file naming convention "none". For  $P$ , also  
 156 the number of wet days is adjusted, according to the description in Section 3.3, using the reanalysis anomalies as a predictor.

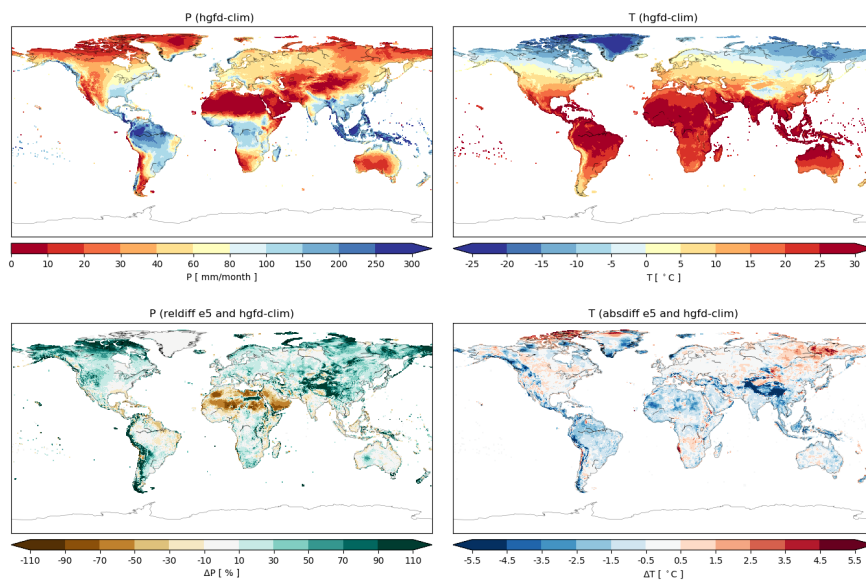


**Figure 4.** The baseline HydroGFD3 annual mean climatology for  $P$  (top left) and  $T$  (top right). The bottom row shows the bias of the e5 reanalysis for each variable.

157 A closer to real-time product is possible, with the daily time step cpcp and cpcpt products being available with a two day  
158 latency, and e5t available at five day latency. The adjustment of the e5t data is then based on the latest available 30 days,  
159 synchronized between the data sets, and is therefore called "Trailing".

#### 160 4.1 Operational aspects

161 The HydroGFD3 data sets are updated at regular intervals. The "extended" period is updated each month, as new e5 and other  
162 data sets become available. Each tier works independently, and can therefore become available at different times.

163 The "near real-time" period is updated at earliest five days into the new month, when e5t is available. By then, the cpcp  
164 and cpcpt products are generally available, but gpcpf normally needs a few days more. Tier 3 needs no additional data sets,  
165 and is available together with e5t, but is produced at the calendar month timestep like the other products. The priority order is  
166 independent for each variable, and goes from Tier 1–3.

167 Finally, the "Trailing" updates are performed along with e5t and cpcp and cpcpt updates, and is normally available at a five  
168 days time lag.



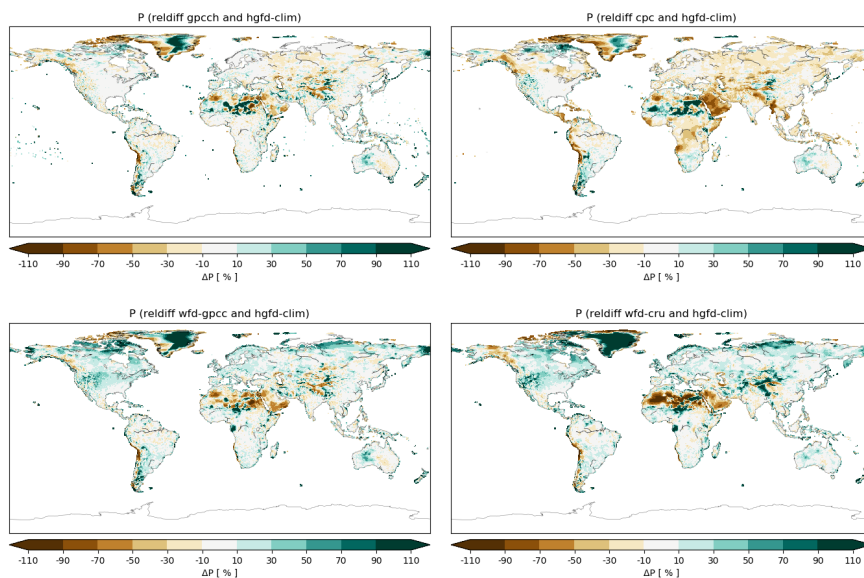


**Figure 5.** Relative difference of data sets to the HydroGFD3 annual mean  $P$  climatology for the period 1980–2009; gpcc (top left), cpcp (top right), wfd-gpcc (bottom left) and wfd-cru (bottom right).

## 169 5 Results

### 170 5.1 Climatology

171 The climatological period of HydroGFD3 is set to 1980–2009, and is consistently used in this section. Figure 4 presents the  
172 annual mean climatology of HydroGFD for both  $P$  and  $T$ , as well as the bias of the e5 reanalysis. e5 has in general a wet and  
173 cold bias in mountainous regions in most of the world. The Arctic is generally wetter and warmer in e5; note that Greenland  $P$   
174 is bias free per definition since the HydroGFD3 climatology uses e5 there. The tropics are generally drier and colder in e5.

175 Figures S1–S4 show the seasonal HydroGFD3 climatology and biases of e5. The bias patterns are rather stable across the  
176 seasons, although the magnitude changes somewhat. Most striking are the relative changes in western Africa in the December–  
177 February period, but this is the dry period there and the relative changes are therefore comparing low numbers which tend to  
178 exaggerate the absolute term differences.

179 We also compare the HydroGFD3 climatologies to other data sets, mainly with a focus on data with daily time steps that  
180 could be used equally for the historical period, but also to gpcc, which is the main background data set for anomalies in the  
181 historical period. Figure 5 shows the annual mean difference in  $P$  of gpcc, cpcp, wfd-gpcc, and wfd-cru to the HydroGFD3  
182 climatology. Differences to gpcc are generally within +/- 10 %, except for parts of the Andes mountain range, the Canadian  
183 Arctic, the dry north of Africa, the Himalayan plateau, and Greenland. The cpcp data set is generally drier, especially in the  
184 Arabian peninsula. wfd-gpcc and wfd-cru are both generally wetter than the HydroGFD3 climatology, especially in the cold  
185 seasons (see Fig. S5–S8). This is due to the gauge corrections applied in the data, which is also the reason for wfd-gpcc not

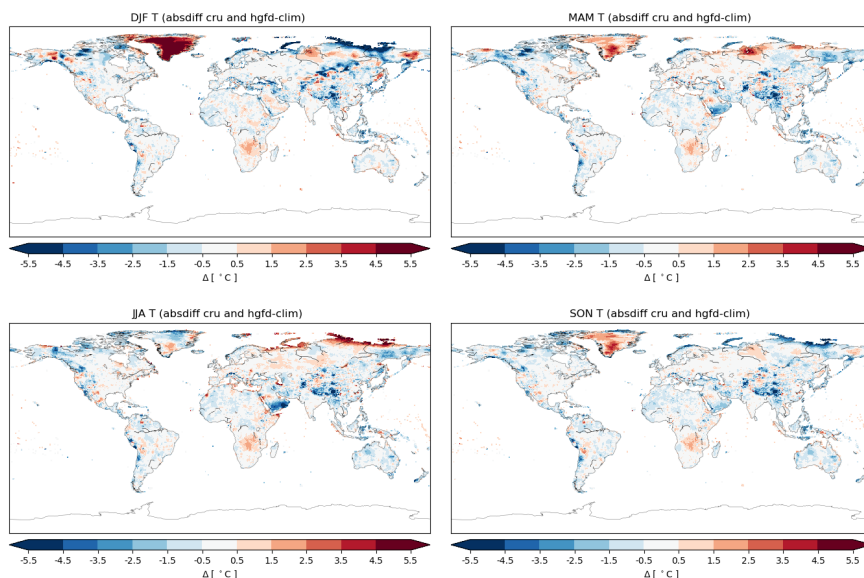


**Figure 6.** Absolute difference  $T$  climatology for the period 1980–2009 between cru and HydroGFD3 for each season (top left) December–February, (top right) March–May, (bottom left) June–August, and (bottom right) September–November.

186 being identical to gpch, which it is based on. However, the two wfd data sets also tend to be drier in very dry areas, which is  
187 likely due to the direct use of the number of rain days from the CRU data set. An incompatibility between  $P$  and no observed  
188 wet days can act to remove  $P$  completely for some months, and therefore making a drier data set. Seasonal differences (Fig. S5–  
189 S8) show similar patterns as the annual mean for most of the regions, but can also differ substantially in some regions. One  
190 region that stands out is southern Africa in JJA, where both gpch and cpcp shows much wetter conditions (Fig. S7).

191 For  $T$ , we compare to cru only, since cpct is used to build the climatology, and wfd-cru is adjusted to cru and is per definition  
192 identical regarding climatology. Fig. 6 shows the absolute difference of cru and the HydroGFD3 climatology for each season  
193 of the climatological year. The largest differences are in the Arctic region where gauge availability is low. In other regions,  
194 such as central-south Africa, the Himalayan plateau, and other orographic regions, the differences are very consistent over all  
195 seasons, with deviations up to a few degrees Celsius. This makes us suspect that they are due to difference in the elevation used  
196 for the different data sets. The cpct data set does not come with any information on the elevations used. The use of anomalies  
197 from the cru and cpct in constructing the final data set removes such effects, but the climatological difference remains.

## 198 5.2 Distributions

199 Figure 7 shows the PDFs for the complete time period 1980–2009 for  $P$ , and for each of the data sets e5, hgfd3, cpcp, wfd-  
200 cru and wfd-gpcc. In these plots, the spread between the coloured lines representing direct observations or e5 adjusted to  
201 observations, can be interpreted as indicators of the uncertainty in the observed state. Many regions show fairly high agreement  
202 between the datasets, including the e5 original data. In some regions, there is a large spread in the observations, and e5 is



203 somewhere in between, e.g. in ALA, GRL, TIB, and SAH. However, in other regions e5 is deviating significantly in part of the  
204 distribution, such as in SSA and WAF moderate intensities, AMZ and EAF extreme intensities.

205 HydroGFD3 tends to have higher extremes than other datasets. This is partly a resolution effect due to the 0.25 degree  
206 resolution of HydroGFD, and 0.5 degree of the other data sets used here. A coarser resolution will move all higher intensities  
207 toward the lower intensities (to the left in the PDF plots). That the effect differs between regions is because the extremes are  
208 also modulated by the magnitude of the applied correction, i.e. the applied scaling. A scaling factor above one will increase  
209 the extremes, and below one will decrease them. The baseline climatology therefore has an impact on the extremes. Also the  
210 wet-days calculation of HydroGFD3 can affect the results, and we find that the dry regions, e.g. SAH and MED, has more  
211 dry days in HydroGFD3 than in the other data sets. When e5 only gives few  $P$  days, while the observational anomaly is  
212 high, the scaling factor can become very large, and the only process to limit this is the upper limit of 1500 mm/day, which is  
213 seldom reached. The wfd-gpcc, which has a similar methodology as HydroGFD3, still has lower extremes. Besides the above  
214 mentioned under-catch corrections, the lower extremes may be due to the upper threshold applied to each hour, as can be seen  
215 in the original wfd-code in the CDS-catalogue (<https://doi.org/10.24381/cds.20d54e34>).

216 For  $T$ , the general shapes of the PDFs agree across all data sets and regions. However, there are sometimes substantial  
217 differences between e5 and the observational data sets. Typically, e5 displays issues around 0 °C, which is common in global  
218 models and related to melting conditions. There are also seasonal offsets outside the range of the observations. HydroGFD3  
219 remains fairly close to cpct and wfd-cru in most cases. Orographic effects on the  $T$  was not accounted for in this comparison,  
220 which can explain some of the differences in regions with varying orography such as TIB.

### 221 5.3 Temporal trends

222 To get an impression of the temporal trends, and to identify potential issues in the time series, we also investigate the time series  
223 as an average over the Giorgi regions. To emphasize differences between the data sets, we discuss mainly differences relative  
224 to a common reference, here chosen to be e5. In other words, we present the inverse bias of e5 compared to each observational  
225 source.

226 Figure 9 shows the results for  $P$  for the period 1980–2019, and the absolute values are shown in Fig. S9. Note that wfd-gpcc  
227 ends in 2016, wfd-cru ends in 2018, and gpccm and gpccfg are only available for the last years. The most striking feature is  
228 the strong deviations of cpct for many of the regions. It also varies significantly with time by changing variance, e.g. in SEA,  
229 changing mean value, e.g. in CAS, SAS, and AMZ. In some years, there are significant offsets compared to surrounding years,  
230 e.g. in 2014 in NEU, NEE, CAS and MED. Likely, these issues are due to variations in the underlying station network, but we  
231 have not verified this. wfd-gpcc and wfd-cru display stronger anomalies over the annual cycle in the colder regions compared to  
232 other data sets. This is likely due to the undercatch corrections which are larger for snowy conditions. As expected, HydroGFD3  
233 follows the general trends of wfd-gpcc, and the other data sets have similar trends, besides the cpct deviations just discussed.  
234 The gpccm and gpccf has similar mean and variance as gpcc in the overlapping period, and shows generally consistent  
235 behavior for the later years. Although, some larger anomalies occur in, e.g., CAN, CAM, SQF, and SAH.

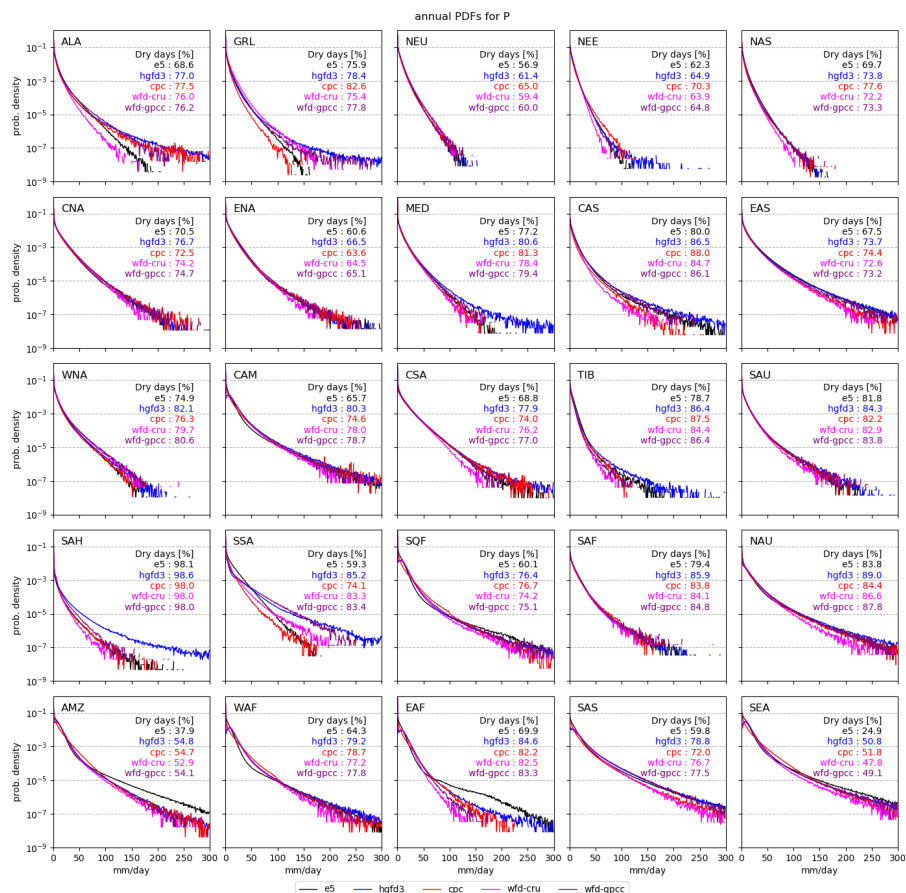


**Figure 7.**  $P$  PDFs of each Giorgi region for the data sets with daily output data in the period 1980–2009. The table in each plot states the percentage of dry days for each data set, i.e. the percentage of data in the first bin of 0–1 mm/day.

236 For  $T$ , the anomalies to e5, see Fig. 10 (and Fig. S10), retain a clear annual cycle in many regions. Sometimes, the annual  
 237 cycle is mainly for wfd-cru (e.g. NEU, TIB, SAS), but often for all data sets. HydroGFD3 and cpct are in general close to each  
 238 other, because of the HydroGFD3 climatology reducing the offset to zero. However, cpct has some clear "break points" in its  
 239 time series in some regions. For example, in NEU, there is a marked change in the magnitude of the anomalies from about 0  
 240 to 0.5 °C to -0.5 to 0.5 °C about year 2006. A similar change about that time is visible also for EAS, GRL, MED, SAS, and  
 241 NAU. Because the climatologies are calculated for the period 1980–2009, part of these changes are included with the earlier  
 242 weaker variability. HydroGFD3 is based on cru anomalies pre-2017, but from 2017 on, also its variability is subjected to the  
 243 changes in cpct.

244 Some regions display a significant offset between the data sets, such as SEA, CSA, MED, TIB, and SAS, with cru having  
 245 generally lower  $T$ s. Interestingly, changes in cpct after 2006 often act to reduce the offset to cru.

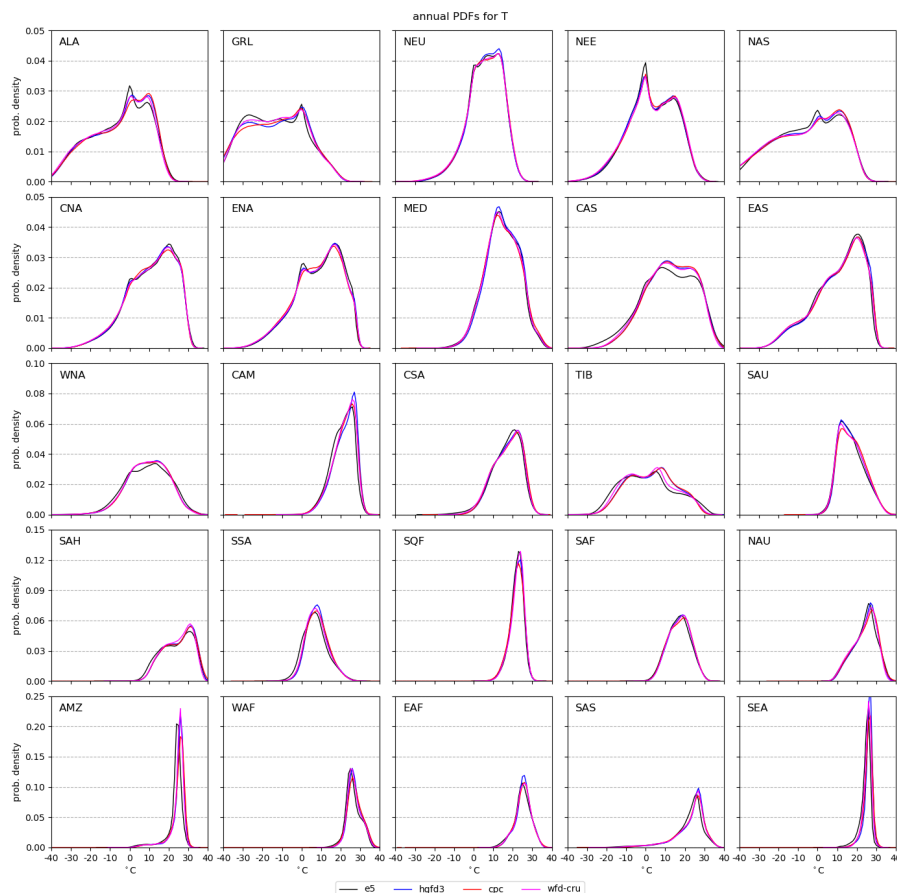


**Figure 8.** *T* PDFs of each Giorgi region for the data sets with daily output data in the period 1980–2009.

#### 246 5.4 Extending to near real-time

247 The near real-time products, in Fig. 3 called "trailing", use the daily updates of the cpcp and cpct observations. They are  
248 therefore subject to the quality of the cpc products, and the changes in time as discussed in the previous section. This product  
249 follows HydroGFD3 fairly closely to that shown in Fig. 9 and 10, as the main version Tier 2 is also based on cpcp and cpct,  
250 but with corrections at calendar months.

251 In addition, also the "none" products are created with the trailing time window. These only replace the e5 climatology with  
252 that of HydroGFD3, and is the simplest form of corrections of the mean. They act as the last failover option in the production  
253 chain, before defaulting to un-corrected e5 data. We do not present this product in the time series plots, since it would only  
254 constitute a constant annual cycle offset in comparison to e5.

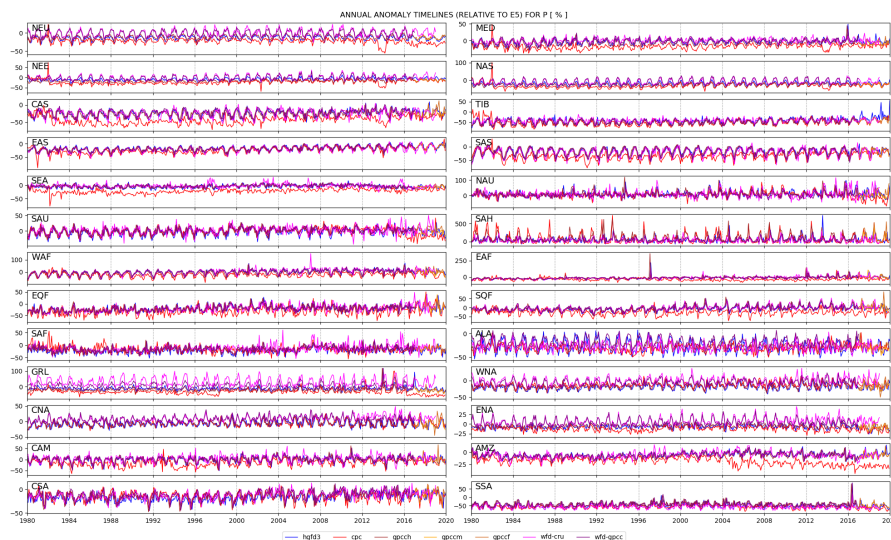


**Figure 9.** *P* anomalies for all data sets, averaged over the Giorgi regions for all valid land data points. The anomalies are relative to the e5 data set, and is evaluated for each single month.

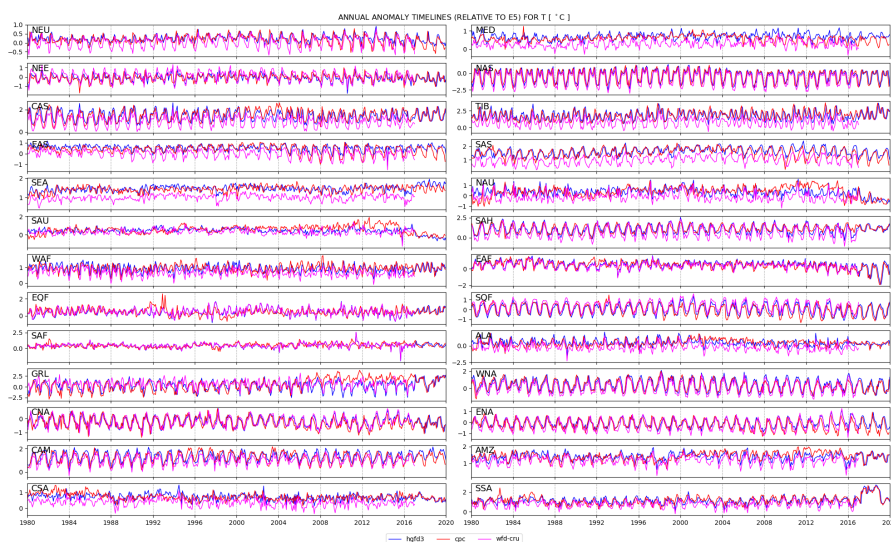


**Figure 10.** *T* anomalies for all data sets, averaged over the Giorgi regions for all valid land data points. The anomalies are relative to the e5 data set, and is evaluated for each single month.

## 255 6 Discussion

256 Compared to similar data sets based on reanalysis, such as WFD and MSWEP, HydroGFD3 differs in that it has its own  
257 climatological background, and performs the corrections based on anomalies of that same climatological time period. The



258 reason for using this method, as to be able to switch datasets closer to real-time, without "jumps" in the time series. This works  
259 well as long as the real-time data set retains its climatological state, which seems to be the case for gpccm and gpccf compared  
260 to gpccch. However, cpct and cpcp both cause issues due to changes in the time series towards the end of the time period, about  
261 year 2006. The bias of e5 is still reduced, which brings validity to the method.

262 HydroGFD3 has generally higher extremes than the other analyzed data sets. This is especially so in drier regions where an  
263 interplay between the estimation of the number of wet days and the scaling causes fewer wet days and larger scaling factors. In  
264 effect, this leads to enlarging the tail of the distribution. It is possible to restrict the scaling by only allowing the scaling factor  
265 to be a few times the original value, but such restrictions would in turn impact on the monthly mean. A potential method would  
266 be to "borrow"  $P$  from adjacent grid points on e5's excessive dry days, and thereby reducing the scaling factors. This topic is  
267 being investigated for future updates of the methodology.

268 The regional analysis shows clearly that the observational data sets give substantially different results in some regions.  
269 Diverse results are more common in data sparse regions or in regions where data are not generally available to all data sets. It is  
270 therefore difficult to determine which is closer to the truth in a global assessment like this, and more detailed regional studies,  
271 such as Fallah et al. (2020), are needed.

272 The current main usage of the data set is to initialize different HYPE forecasting models around the world, e.g. in Europe  
273 (Hundecha et al., 2016), the Niger river (Andersson et al., 2017), and world-wide (Arheimer et al., 2020). This has influenced  
274 some of the choices for the setup, such as the use of only the ERA5 reanalysis model, among other reanalysis systems used  
275 in e.g. the MSWEP data set (Beck et al., 2017). The forecasts produced by these hydrological models are primarily using the  
276 ECMWF deterministic medium range forecasts, or the probabilistic SEAS5 seasonal forecasts, which both use the same model  
277 as e5. The priority order of the different redundancy options, i.e. the Tiers 1–3, is based on experience with using the different  
278 data sources for our forecasts, with impact from both availability for a given month as well as experienced longer interruptions.

## 279 7 Conclusions

280 The HydroGFD3 methodology of correcting the e5 reanalysis model toward an observational reference, along with the resulting  
281 data sets were presented. We conclude that the data sets compare well with existing similar data sets.

282 The main new features of HydroGFD3 are:

- 283 – Higher spatial resolution of 0.25 degrees.
- 284 – Near real-time corrected data until five days from now, i.e. following the continuous updates e5 + e5t time period.
- 285 – Temporal coverage from 1979, and will be extended back to 1950 along with the extended e5 data expected during 2020.
- 286 – Multiple redundancy options to avoid halting production when single data sets are delayed.

287 The data is freely available for the period 1979–2019, and by subscription for the real-time products. See Section 8 for  
288 details.



289 **8 Data availability**

290 A historical period, ranging from February 1979 to December 2019, is available as open source from the ZENODO repository  
291 at [doi:10.5281/zenodo.3871707](https://doi.org/10.5281/zenodo.3871707). For years prior to 2017, cru and gpccm are used as reference data for  $T$  and  $P$ , respectively.  
292 The following years use instead gpccm and cpct reference data.

293 Real-time updates of the data set are available for a processing charge via subscriptions. Please make a request here:  
294 <https://hypeweb.smhi.se/buy-water-services/data-subscription/> and make sure to mention the data set name "HydroGFD3".

295 *Acknowledgements.* The authors would like to thank the EU and the Swedish Research Council Formas for funding, in the frame of the  
296 GlobalHydroPressure project financed under the 2017 Joint Call of Water JPI (IC4WATER).





## 297 References

- 298 Andersson, J. C., Ali, A., Arheimer, B., Gustafsson, D., and Minoungou, B.: Providing peak river flow statistics and forecasting in the Niger  
299 River basin, *Phys. Chem. Earth A/B/C*, 100, 3–12, <https://doi.org/10.1016/j.pce.2017.02.010>, 2017.
- 300 Arheimer, B., Pimentel, R., Isberg, K., Crochemore, L., Andersson, J. C. M., Hasan, A., and Pineda, L.: Global catchment mod-  
301 elling using World-Wide HYPE (WWH), open data, and stepwise parameter estimation, *Hydrol. Earth Syst. Sci.*, 24, 535–559,  
302 <https://doi.org/10.5194/hess-24-535-2020>, 2020.
- 303 Ashouri, H., Hsu, K.-L., Sorooshian, S., Braithwaite, D. K., Knapp, K. R., Cecil, L. D., Nelson, B. R., and Prat, O. P.: PERSIANN-CDR:  
304 Daily Precipitation Climate Data Record from Multisatellite Observations for Hydrological and Climate Studies, *Bull. Amer. Meteor.*  
305 *Soc.*, 96, 69–83, <https://doi.org/10.1175/bams-d-13-00068.1>, 2015.
- 306 Beck, H. E., van Dijk, A. I. J. M., Levizzani, V., Schellekens, J., Miralles, D. G., Martens, B., and de Roo, A.: MSWEP: 3-hourly  
307 0.25° global gridded precipitation (1979–2015) by merging gauge, satellite, and reanalysis data, *Hydrol. Earth Syst. Sci.*, 21, 589–615,  
308 <https://doi.org/10.5194/hess-21-589-2017>, 2017.
- 309 Berg, P., Donnelly, C., and Gustafsson, D.: Near-real-time adjusted reanalysis forcing data for hydrology, *Hydrol. Earth Syst. Sci.*, 22,  
310 989–1000, <https://doi.org/10.5194/hess-22-989-2018>, 2018.
- 311 Chen, M., Shi, W., Xie, P., Silva, V. B. S., Kousky, V. E., Wayne Higgins, R., and Janowiak, J. E.: Assessing objective techniques for  
312 gauge-based analyses of global daily precipitation, *J. Geophys. Res. Atm.*, 113, D04 110, <https://doi.org/10.1029/2007JD009132>, 2008.  
313 CPCtemp: <https://www.esrl.noaa.gov/psd/data/gridded/data.cpc.globaltemp.html>, 2017.
- 314 Cucchi, M., Weedon, G. P., Amici, A., Bellouin, N., Lange, S., Schmied, H. M., Hersbach, H., and Buontempo, C.: WFDE5: bias adjusted  
315 ERA5 reanalysis data for impact studies, *Earth Syst. Sci. Data Discuss.*, pp. 1–32, <https://doi.org/10.5194/essd-2020-28>, 2020.
- 316 Fallah, A., Rakhshandehroo, G. R., Berg, P., O, S., and Orth, R.: Evaluation of precipitation datasets against local observations in southwestern  
317 Iran, *Int. J. Climatol.*, <https://doi.org/10.1002/joc.6445>, 2020.
- 318 Fan, Y. and Van den Dool, H.: A global monthly land surface air temperature analysis for 1948–present, *J. Geophys. Res. Atm.*, 113, D1,  
319 <https://doi.org/10.1029/2007JD008470>, 2008.
- 320 Funk, C., Peterson, P., Landsfeld, M., Pedreros, D., Verdin, J., Shukla, S., Husak, G., Rowland, J., Harrison, L., Hoell, A., and Michaelsen,  
321 J.: The climate hazards infrared precipitation with stations—a new environmental record for monitoring extremes, *Sci. Data*, 2,  
322 <https://doi.org/10.1038/sdata.2015.66>, 2015a.
- 323 Funk, C., Verdin, A., Michaelsen, J., Peterson, P., Pedreros, D., and Husak, G.: A global satellite-assisted precipitation climatology, *Earth*  
324 *Syst. Sci. Data*, 7, 275–287, <https://doi.org/10.5194/essd-7-275-2015>, 2015b.
- 325 Giorgi, F. and Bi, X.: Updated regional precipitation and temperature changes for the 21st century from ensembles of recent AOGCM  
326 simulations, *Geophys. Res. Lett.*, 32, <https://doi.org/10.1029/2005gl024288>, 2005.
- 327 Harris, I. C. and Jones, P. D.: CRU TS4.03: Climatic Research Unit (CRU) Time-Series (TS) version 4.03 of high-resolution gridded data of  
328 month-by-month variation in climate (Jan. 1901– Dec. 2018), <https://doi.org/10.5285/10D3E3640F004C578403419AAC167D82>, 2019.
- 329 Hersbach, H., Bell, B., Berrisford, P., Hirahara, S., Horányi, A., Muñoz-Sabater, J., Nicolas, J., Peubey, C., Radu, R., Schepers, D., Simmons,  
330 A., Soci, C., Abdalla, S., Abellan, X., Balsamo, G., Bechtold, P., Biavati, G., Bidlot, J., Bonavita, M., Chiara, G., Dahlgren, P., Dee,  
331 D., Diamantakis, M., Dragani, R., Flemming, J., Forbes, R., Fuentes, M., Geer, A., Haimberger, L., Healy, S., Hogan, R. J., Hólm, E.,  
332 Janisková, M., Keeley, S., Laloyaux, P., Lopez, P., Lupu, C., Radnoti, G., Rosnay, P., Rozum, I., Vamborg, F., Villaume, S., and Thépaut,  
333 J.-N.: The ERA5 global reanalysis, *Quart. J. Roy. Meteor. Soc.*, 146, 1999–2049, <https://doi.org/10.1002/qj.3803>, 2020.



- 334 Huebener, H. and Körper, J.: Changes in Regional Potential Vegetation in Response to an Ambitious Mitigation Scenario, *J Environ Prot*, 04,  
335 16–26, <https://doi.org/10.4236/jep.2013.48a2003>, 2013.
- 336 Hundecha, Y., Arheimer, B., Donnelly, C., and Pechlivanidis, I.: A regional parameter estimation scheme for a pan-European multi-basin  
337 model, *J. Hydrol. Regional Studies*, 6, 90–111, <https://doi.org/10.1016/j.ejrh.2016.04.002>, 2016.
- 338 Joyce, R. J., Janowiak, J. E., Arkin, P. A., and Xie, P.: CMORPH: A Method that Produces Global Precipitation Estimates from Passive  
339 Microwave and Infrared Data at High Spatial and Temporal Resolution, *J. Hydrometeorol.*, 5, 487–503, [https://doi.org/10.1175/1525-7541\(2004\)005<0487:camtpg>2.0.co;2](https://doi.org/10.1175/1525-7541(2004)005<0487:camtpg>2.0.co;2), 2004.
- 341 Lindström, G., Pers, C., Rosberg, R., Strömqvist, J., and Arheimer, B.: Development and test of the HYPE (Hydrological Pre-  
342 dictions for the Environment) model - A water quality model for different spatial scales, *Hydrol. Res.*, 41.3-4, 295–319,  
343 <https://doi.org/10.2166/nh.2010.007>, 2010.
- 344 Schneider, U., Becker, A., Finger, P., Meyer-Christoffer, A., and Ziese, M.: GPCC Full Data Monthly Version 2018.0 at 0.25: Monthly Land-  
345 Surface Precipitation from Rain-Gauges built on GTS-based and Historic Data, [https://doi.org/10.5676/DWD\\_GPCC/FD\\_M\\_V2018\\_025](https://doi.org/10.5676/DWD_GPCC/FD_M_V2018_025),  
346 2018a.
- 347 Schneider, U., Becker, A., Finger, P., Meyer-Christoffer, A., and Ziese, M.: GPCC Monitoring Product Version 6.0 at  
348 1.0: Near Real-Time Monthly Land-Surface Precipitation from Rain-Gauges based on SYNOP and CLIMAT Data,  
349 [https://doi.org/10.5676/DWD\\_GPCC/MP\\_M\\_V6\\_100](https://doi.org/10.5676/DWD_GPCC/MP_M_V6_100), 2018b.
- 350 Stillman, S. and Zeng, X.: Development of a 0.5° global monthly raining day product from 1901 to 2010, *Geophys. Res. Lett.*, 43, 9704–9711,  
351 <https://doi.org/10.1002/2016gl070244>, 2016.
- 352 Weedon, G., Gomes, S., Viterbo, P., Shuttleworth, W., Blyth, E., Österle, H., Adam, C., Bellouin, N., Boucher, O., and Best, M.: Creation  
353 of the watch forcing data and its use to assess global and regional reference crop evaporation over land during the twentieth century, *J.*  
354 *Hydrometeorol.*, 12, 823–848, <https://doi.org/10.1175/2011JHM1369.1>, 2011.
- 355 Weedon, G. P., Balsamo, G., Bellouin, N., Gomes, S., Best, M. J., and Viterbo, P.: The WFDEI meteorological forcing data set: WATCH  
356 Forcing Data methodology applied to ERA-Interim reanalysis data, *Water Resour. Res.*, 50, 7505–7514, 2014.